A PDF-Based Model for Boundary Layer Clouds. Part I: Method and Model Description

JEAN-CHRISTOPHE GOLAZ

Department of Atmospheric Science, Colorado State University, Fort Collins, Colorado

VINCENT E. LARSON

Atmospheric Science Group, Department of Mathematical Sciences, University of Wisconsin–Milwaukee, Milwaukee, Wisconsin

WILLIAM R. COTTON

Department of Atmospheric Science, Colorado State University, Fort Collins, Colorado

(Manuscript received 14 November 2001, in final form 28 May 2002)

ABSTRACT

A new cloudy boundary layer single-column model is presented. It is designed to be flexible enough to represent a variety of cloudiness regimes—such as cumulus, stratocumulus, and clear regimes—without the need for case-specific adjustments. The methodology behind the model is the so-called assumed probability density function (PDF) method. The parameterization differs from higher-order closure or mass-flux schemes in that it achieves closure by the use of a relatively sophisticated joint PDF of vertical velocity, temperature, and moisture. A family of PDFs is chosen that is flexible enough to represent various cloudiness regimes. A double Gaussian family proposed by previous works is used. Predictive equations for grid box means and a number of higher-order turbulent moments are advanced in time. These moments are in turn used to select a particular member from the family of PDFs, for each time step and grid box. Once a PDF member has been selected, the scheme integrates over the PDF to close higher-order moments, buoyancy terms, and diagnose cloud fraction and liquid water. Since all the diagnosed moments for a given grid box and time step are derived from the same unique joint PDF, they are guaranteed to be consistent with one another. A companion paper presents simulations produced by the single-column model.

1. Introduction

Boundary layer clouds play an important role in the energy and hydrological cycle of the atmosphere. Slingo (1990) showed, using a general circulation model, that small changes in low-level cloud amount or cloud properties could significantly affect the global radiation budget. Using satellite observations, Hartmann et al. (1992) demonstrated that low-level clouds, with 60% of the total cloud radiative forcing, are the largest contributors to the planetary net cloud forcing. Among low-level clouds, marine stratocumulus clouds exert a large effect on the radiative budget. They sharply reduce the net incoming shortwave radiation owing to their high albedo compared to the underlying ocean surface, while at the same time leaving the longwave radiation to space essentially unaffected, owing to their low altitude. Since sheets of stratocumulus often break up into cumulus layers with much lower albedo, it is important to be able to accurately predict which cloud regime is present.

Because boundary layer clouds have characteristic sizes that are much smaller than grid boxes used in large-scale models, such as general circulation models and mesoscale forecast models, they must be parameterized. Their incorporation in present-day numerical models continues to pose a significant challenge. Parameterizations have frequently been developed for specific cloudiness regimes. With this approach, boundary layer clouds are first classified into various categories, such as stratocumulus clouds or shallow cumulus clouds, and then specific parameterizations are developed for each regime. The categorization into regimes is, however, somewhat arbitrary, and leads to the difficult problem of interfacing the various components to obtain a general-purpose parameterization.

One class of parameterization used for boundary layer clouds includes higher-order turbulence closure models. As of yet, no single turbulence closure model has succeeded in modeling both cumulus and stratocumulus regimes without case-specific adjustments. For instance,

Corresponding author address: Jean-Christophe Golaz, Naval Research Laboratory, Marine Meteorology Division, 7 Grace Hopper Ave., Stop 2, Monterey, CA 93943-5502.
E-mail: golaz@nrlmry.navy.mil

Bougeault (1981a,b) developed a closure model with prognostic equations for all the turbulent moments up to the third order. This higher-order closure scheme was coupled with a statistical representation of the subgrid-scale cloudiness. He used the scheme to simulate a trade wind cumulus layer observed during the Puerto Rico Experiment. However, in order to model a different regime like a marine stratocumulus layer, Bougeault (1985) changed the statistical cloudiness scheme and the representation of the mixing length from the ones in his original model.

Low-order closure models form another category of parameterization. They typically only carry a prognostic equation for the turbulence kinetic energy and close all other second-order moments diagnostically. These schemes have been used quite successfully to simulate stratocumulus layers (e.g., Duynkerke and Driedonks 1987, 1988; Bechtold et al. 1992). However, Bechtold et al. (1995) showed that the closure assumptions had to be modified in order to simulate trade wind cumulus with a low-order model. They found that a statistical subgrid-scale cloudiness scheme using a Gaussian distribution was well suited for stratocumulus clouds but that a positively skewed distribution was necessary to represent cumulus convection, implying that different variants of the subgrid-scale cloudiness scheme were needed for different cloud regimes, similar to the findings of Bougeault (1985).

Mass-flux models represent another type of cloud parameterization. Following Arakawa and Schubert (1974), such models simulate subgrid-scale convection by representing cloud ensembles as one-dimensional plumes embedded in the environment. Some large-scale models have incorporated mass-flux parameterizations for shallow convection, such as for trade wind cumulus clouds (e.g., Tiedtke 1989; Gregory and Rowntree 1990).

Since mass-flux parameterizations typically only handle convective clouds, models incorporating them include alternate schemes to account for other boundary layer cloud regimes. Lock et al. (2000) presented a parameterization consisting of various schemes coupled together, including a mass-flux convection scheme for cumulus layers, a nonlocal eddy viscosity scheme for mixed layers, and a cloud-top entrainment parameterization. A total of six possible boundary layer regimes are identified, and a set of rules based on stability of the mean profiles and parcel buoyancy is used to activate the appropriate components of the parameterization at any given time. Although they found that the parameterization was ''capable of switching reasonably smoothly and realistically between the different regimes,'' it has not been fully established that a simple set of rules can trigger the correct scheme under the full set of conditions.

Lappen and Randall (2001a,b,c) simulated various cloudiness regimes with a single scheme that unifies mass-flux and higher-order closure approaches. The mass-flux approach was used to decompose the boundary layer into updraft and downdraft plumes, and this decomposition was related in turn to the turbulent moments as originally proposed by Randall et al. (1992). The mass-flux decomposition is equivalent to assuming a double delta function probability density function (PDF). Lappen and Randall improved upon this distribution by adding subplume variability in the up- and downdrafts. Their new scheme was applied to simulate a dry convective boundary layer, a trade wind cumulus layer, and a stratocumulus-topped layer. The simulation of the dry convective layer and the stratocumulus case agreed well with observations, but the trade wind cumulus simulation produced cloud fraction and liquid water values that were too large compared to the observations.

In the present paper, we propose a new scheme that is different from either mass-flux schemes or traditional higher-order moment schemes. The focus of our scheme is not the separate prediction of cumulus mass-flux, turbulent moments, cloud cover, and other desired predictands per se. Rather, the focus is the prediction of the joint PDF of vertical velocity, temperature, and moisture content. This joint PDF varies in space and evolves in time. The joint PDF can be viewed as a more fundamental quantity than the mass flux, turbulent moments, and cloud cover, because the latter quantities can be diagnosed once the joint PDF is known. Explicitly predicting the shape of the PDF is computationally expensive, so we instead assume a double Gaussian functional form for the PDF. The problem then reduces to the selection of a particular member from the family of PDFs for each grid box and time step. This method, frequently referred to as the ''assumed PDF method,'' has been applied in the engineering community to study combustion in fluids (e.g., O'Brien 1980; Frankel et al. 1993; Bray and Libby 1994; Cook and Riley 1994). In the atmospheric sciences, PDFs have been used in the past to parameterize subgrid-scale moisture variations and thereby account for partial cloud cover (e.g., Sommeria and Deardorff 1977; Mellor 1977; Bougeault 1981a; Chen and Cotton 1987).

Our parameterization can be regarded as a traditional higher-order closure model that uses a new closure based on a double Gaussian family of PDFs. Alternatively, our parameterization can be regarded as an extension of Lappen and Randall's model, in which the double delta function PDF they used for closure is generalized to a double Gaussian PDF. The generalization is inspired by the fact that Larson et al. (2002) evaluated the performance of several families of joint PDFs and found that atmospheric PDFs resemble double Gaussians more than double delta functions.

This paper is organized as follows. Section 2 gives a general overview of the assumed PDF method, its use for building a boundary layer parameterization, as well as some of its advantages and disadvantages. In section 3, we describe a new single-column model constructed

using the assumed PDF method. We summarize the choice of the family of PDFs and the predictive moment equations. Details of the numerical implementation are also presented. We finish with some concluding remarks. Results obtained with the parameterization for a variety of boundary layer regimes are presented in a comparison paper (Golaz et al. 2002, hereafter Part II).

2. The assumed PDF method

a. General description

We denote the joint PDF of vertical velocity w, liquid water potential temperature θ_l, and total specific water content q_t by $P(w, \theta_l, q_t)$. If $P(w, \theta_l, q_t)$ is a joint PDF, then $P(w, \theta_l, q_t)\, dw\, d\theta_l\, dq_t$ is the probability of obtaining a value of (w, θ_l, q_t) within the range $(w - dw/2) < w < (w + dw/2)$,$(\theta_l - d\theta_l/2) < \theta_l < (\theta_l + d\theta_l/2)$, and $(q_t - dq_t/2) < q_t < (q_t + dq_t/2)$ at a specific location and time. For the purpose of this work, we are interested in the joint PDF associated with a particular model grid box and time step. The joint PDF then becomes a characterization of the unresolved subgrid variations that occur within this particular box. However, the PDF does not provide any information about the spatial organization of this variability within the box of interest.

Because directly predicting the full subgrid-scale joint PDF is computationally too expensive, the assumed PDF method requires the PDFs to lie within a preselected family of PDFs, such as the multivariate Gaussian. Although this family of PDFs is not recommended for large-scale grid boxes (Larson et al. 2002), it serves as a familiar example. The Gaussian shape defines a family of joint vertical velocity, temperature and moisture PDFs whose positions, widths, and correlations vary. This particular family depends on nine PDF parameters: three for the positions of the Gaussian along the three dimensions w, θ_l, q_t; three for their respective widths; and three for the correlations between the dimensions. Within this family of PDFs, one needs to select a particular member—identified by its values of the nine PDF parameters—for each grid box and time step.

How can we determine the PDF parameters? To do so, we use the numerical model to predict moments in each grid box and require the PDF's moments to match the predicted moments. For our example of the multivariate Gaussian distribution, a logical choice of moments to predict would be the means $\overline{w}$, $\overline{\theta}_l$, $\overline{q}_t$, the variances $\overline{w'^2}$, $\overline{\theta_l'^2}$ $\overline{q_t'^2}$, and the correlations $\overline{w'\theta_l'}$, $\overline{w'q_t'}$, $\overline{\theta_l'q_t'}$. For this simple example, these moments also happen to be the nine PDF parameters characterizing the PDF family. This is generally not the case, however, and a mapping must then be constructed between the grid box moments and the PDF parameters. Examples of such mappings are described in Larson et al. (2001a, 2002). To predict the needed moments, the assumed PDF method requires that the model include additional prognostic equations for the desired higher-order moments. Mean quantities are typically predicted by atmospheric models. The number of additional equations depends upon the complexity of the chosen family of PDFs, that is, the number of PDF parameters required to characterize the family.

The prognostic moments equations needed are the standard higher-order moment equations based on the Navier–Stokes and advection–diffusion equations (e.g., Stull 1988). These equations contain unclosed higher-order and buoyancy terms. In many models, the higher-order terms are closed by assuming that the quantity of interest diffuses down the gradient of that quantity (e.g., Donaldson 1973; Wyngaard et al. 1974; Lumley and Khajeh-Nouri 1974). This assumption is often poor (Moeng and Wyngaard 1989). The quasi-normal assumption, which expresses the fourth-order correlations in term of the second-order moments assuming Gaussianity, has also been used in numerous third-order closure models (e.g., André et al. 1976a,b). However, the quasi-normal assumption does not require the third-order moments to vanish, as would be required for strict consistency with the Gaussian PDF. The assumptions used to close buoyancy terms are typically inconsistent with the closure of the higher-order moments. For example, Bougeault (1981b) used the quasi-normal assumption to close the fourth-order moments and used a positively skewed PDF to close the buoyancy terms. Cumulus layers typically have positive skewness values, which is inconsistent with the zero skewness assumption of the quasi-normal closure. One of the advantages of the assumed PDF method is that once the joint PDF of w, θ_l, and q_t is known, then any moments or correlations involving these variables can be computed by integration over the PDF. In particular, the unclosed terms that involve only these variables can be computed from the PDF without any additional assumptions. For example, any correlation of the form $\overline{w'^l\theta_l'^m q_t'^n}$—where l, m, n are positive integers–can be computed as follows:

$$\overline{w'^l\theta_l'^m q_t'^n} = \int\int\int (w - \overline{w})^l(\theta_l - \overline{\theta}_l)^m(q_t - \overline{q}_t)^n \times P(w, \theta_l, q_t)dw\, d\theta_l\, dq_t. \quad (1)$$

Cloud fraction and cloud water can be diagnosed directly by integrating over the saturated portion of the PDF. Buoyancy-related moments (involving the virtual potential temperature θ_v') can also be computed directly from the joint PDF and depend on the particular choice of the family of PDFs. For example, Sommeria and Deardorff (1977) and Mellor (1977) proposed formulas for a Gaussian distribution. Using a double delta PDF, Randall (1987) derived an expression for the buoyancy flux that significantly differed from the expressions based on a Gaussian distribution. The higher-order moment equations also contain pressure terms involving correlations between pressure and scalar perturbations.

Because pressure is not included in the PDF, these terms are closed using standard parameterizations (see below).

b. Advantages

The assumed PDF method has some advantages that, in principle, may help address several difficulties confronting parameterizations of boundary layer clouds.

1) *Consistency.* In some schemes, cloud fraction and cloud water content are predicted separately from each other; in other schemes, different closure methods are used for higher-order moments and buoyancy terms (e.g., Bougeault 1981b). When this is the case, there is no guarantee of consistency among the various components forming a parameterization. With the PDF method, in contrast, the prediction of cloud fraction, cloud water, higher-order moments, and buoyancy terms are guaranteed to be internally consistent, since all of them are derived from the same PDF (Lappen and Randall 2001a).
2) *Flexibility.* A PDF parameterization is somewhat modular, with the prognostic equations separated to some degree from the choice of the PDF family. Therefore, the family of PDFs can be changed without having to entirely rewrite a parameterization. This makes the assumed PDF method rather flexible. However, changing the PDF involves rewriting the mapping between the moments and the PDF parameters, and also involves modifying the diagnosis of higher-order moments, buoyancy terms, cloud fraction, and liquid water. If the number of PDF parameters changes from one family of PDFs to another, one also has to add or remove prognostic equations.
3) *Testable empiricism.* The moment equations derived from the Navier–Stokes and advection–diffusion equations are closed using a family of PDFs. This PDF family can be tested and validated against observations. For instance, Larson et al. (2001a, 2002) have tested numerous families of PDFs against aircraft data and large eddy simulations for a variety of boundary layer cloudiness regimes.
4) *Avoiding biases.* In other types of closure, even when cloud fraction is taken into account, systematic biases in cloud and radiative properties remain, due to the neglect of subgrid-scale variability (Cahalan et al. 1994; Rotstayn 2000; Pincus and Klein 2000; Larson et al. 2001b). For instance, the autoconversion process by which cloud droplets grow to drizzle-sized drops is frequently represented using the Kessler autoconversion parameterization (Kessler 1969). If one uses this parameterization and neglects subgrid variability within a grid box, one systematically underpredicts autoconversion in the grid box relative to what one would obtain if subgrid variability were taken into account. But the PDF approximates the subgrid information needed to remove such a bias.
5) *Avoiding trigger functions.* Some parameterization packages contain separate schemes for separate regimes and use trigger functions to activate the correct scheme. For example, Lock et al. (2000) use a mixed-layer scheme for stratocumulus and a separate mass-flux scheme for cumulus. The algorithm then decides which scheme to activate via a set of rules: the trigger function. It is difficult to formulate a sufficiently general trigger function to use under a wide range of conditions. For instance, the transition from stratocumulus to cumulus depends on many factors, including surface latent heat fluxes, surface shear, and drizzle rate (Lenschow 1998). Furthermore, the use of a trigger function introduces an artificially sharp transition between meteorological regimes. However, if one uses the assumed PDF method and chooses a sufficiently general family of PDFs, then one can avoid the use of trigger functions. A single scheme can then be applied to all regimes and can simulate a smooth transition from one regime to another.

c. Disadvantages

The disadvantages of the assumed PDF method are mostly related to the computational cost of implementing a PDF-based parameterization. The computational cost falls into four categories.

1) *Additional prognostic equations.* In the assumed PDF method, the number of prognostic moments must equal the number of free parameters in the chosen family of PDFs. The PDF used for this work needs seven moment equations in addition to the mean equations already prognosed by the host model (see next section). The scheme is therefore computationally more expensive than simpler turbulence kinetic-energy-based schemes used in many models. The added cost is comparable to second-order closure models, but it is considerably less than full third-order models.
2) *Time step.* The addition of prognostic equations for the higher-order moments acts to limit the allowable time step. Typically, time steps of a few seconds have been used in higher-order closure models (e.g., Bougeault 1981b). Through the use of a nested time-stepping scheme presented in section 3c, we were able to increase the main time step to approximately 20 s. This becomes comparable to typical time increments in mesoscale models but is still well below increments used in general circulation models.
3) *Vertical grid spacing.* Because the model must explicitly resolve boundary layer features such as inversions, a relatively fine vertical grid spacing is needed. This limitation is, however, not particular to the assumed PDF method, but applies to many other closure models as well.
4) *Momentum fluxes.* The joint PDF family does not include perturbations involving horizontal winds u'

and v', and as a result the momentum fluxes are currently closed using a traditional downgradient diffusion approach. However, generalizing the PDF to include horizontal winds would add complexity (Lappen and Randall 2001a).

3. Model description

a. Basic equations

This section describes the new boundary layer single-column model, which is based on the assumed PDF method. The PDF family retained for this work is the analytic double Gaussian 1 PDF suggested in Larson et al. (2002). It is a double Gaussian with correlation between θ_l and q_t within each individual Gaussian:

$$P(w, \theta_l, q_t) = aG_1(w, \theta_l, q_t) + (1 - a)G_2(w, \theta_l, q_t), \quad (2a)$$

with

$$G(w, \theta_l, q_t) = \frac{1}{(2\pi)^{3/2}\sigma_{wi}\sigma_{q_{ti}}\sigma_{\theta_{ti}}(1 - r_{q_t\theta_l}^2)^{1/2}} \times \exp\left[-\frac{1}{2}\left(\frac{w - (w_i - \overline{w})}{\sigma_{wi}}\right)^2\right] \times \exp\left\langle -\frac{1}{2(1 - r_{q_t\theta_l}^2)}\left\{\left[\frac{q_t - (q_{ti} - \overline{q}_t)}{\sigma_{q_{ti}}}\right]^2 + \left[\frac{\theta_l - (\theta_{li} - \overline{\theta}_l)}{\sigma_{\theta_{li}}}\right]^2 - 2r_{q_t\theta_l}\left[\frac{q_t - (q_{ti} - \overline{q}_t)}{\sigma_{q_{ti}}}\right]\left[\frac{\theta_l - (\theta_{li} - \overline{\theta}_l)}{\sigma_{\theta_{li}}}\right]\right\}\right\rangle. \quad (2b)$$

This family of PDFs depends on a number of free parameters:

- a is the relative weight of the first Gaussian;
- ψ_1, ψ_2, σ_{ψ_1}, and σ_{ψ_2} are locations and widths of the vertical velocity (w), liquid water potential temperature (θ_l), and total specific water content (q_t) Gaussians;
- $r_{q_t\theta_l}$ is the intra-Gaussian correlation between liquid water potential temperature and total specific water content.

Some examples of double Gaussian PDFs projected on the vertical velocity axis are depicted in Fig. 1. They demonstrate some of the flexibility of the family of PDFs. It can represent symmetric distributions (Figs. 1a and 1b) that could, for instance, occur in stratocumulus layers, but it can also represent skewed distributions. Figure 1f, with its long tail extending on the positive side of the vertical velocity axis, is typical of what might be encountered in a cumulus layer. Although the analytic double Gaussian 1 family cannot reduce to a single Gaussian in w, it does reduce to a single Gaussian in θ_l and q_t when the corresponding fluxes vanish [Eqs. (6) and (7) below].

The PDF parameters used to characterize a particular member from the family of PDFs are obtained analytically from 10 moments. They are the means of vertical velocity $\overline{w}$, liquid water potential temperature $\overline{\theta}_l$, and total water specific humidity $\overline{q}_t$; the second-order moments $\overline{w'\theta_l'}$, $\overline{w'q_t'}$, $\overline{q_t'\theta_l'}$, $\overline{w'^2}$, $\overline{\theta_l'^2}$, $\overline{q_t'^2}$; and the third-order moment of the vertical velocity $\overline{w'^3}$. Because the number PDF parameters (15) is larger than the number of prognostic moments (10), additional assumptions are needed. Complete details are given in Larson et al. (2002). We only briefly outline the methodology to obtain the PDF parameters here. The vertical velocity moments $\overline{w}$, $\overline{w'^2}$, and $\overline{w'^3}$ are used to compute the PDF parameters a, w_1, w_2, σ_{w1}, and σ_{w2}. The width of each Gaussian along the w coordinate is defined as $\sigma_{w1} = \sigma_{w2} = \tilde{\sigma}_w\sqrt{\overline{w'^2}}$. We choose $\tilde{\sigma}_w = 0.4$. The relative weight of each Gaussian a, as well as its locations w_1 and w_2 are obtained by integrating the PDF to obtain expressions for $\overline{w}$, $\overline{w'^2}$, and $\overline{w'^3}$. We define the skewness $\mathrm{Sk}_w \equiv \overline{w'^3}/(\overline{w'^2}^{3/2})$ and find

$$a = \frac{1}{2}\left\{1 - \mathrm{Sk}_w\left[\frac{1}{4(1 - \tilde{\sigma}_w^2)^3 + \mathrm{Sk}_w^2}\right]^{1/2}\right\}, \quad (3)$$

$$\tilde{w}_1 \equiv \frac{w_1 - \overline{w}}{\sqrt{\overline{w'^2}}} = \left(\frac{1 - a}{a}\right)^{1/2}(1 - \tilde{\sigma}_w^2)^{1/2}, \quad (4)$$

$$\tilde{w}_2 \equiv \frac{w_2 - \overline{w}}{\sqrt{\overline{w'^2}}} = -\left(\frac{a}{1 - a}\right)^{1/2}(1 - \tilde{\sigma}_w^2)^{1/2}. \quad (5)$$

The parameters θ_{l1} and θ_{l2} are obtained from the equations for $\overline{\theta}_l$ and $\overline{w'\theta_l'}$:

$$\tilde{\theta}_{l1} \equiv \frac{\theta_{l1} - \overline{\theta_l}}{\sqrt{\overline{\theta_l'^2}}} = -\frac{\overline{w'\theta_l'}/(\sqrt{\overline{w'^2}}\sqrt{\overline{\theta_l'^2}})}{\tilde{w}_2}, \quad (6)$$

$$\tilde{\theta}_{l2} \equiv \frac{\theta_{l2} - \overline{\theta_l}}{\sqrt{\overline{\theta_l'^2}}} = -\frac{\overline{w'\theta_l'}/(\sqrt{\overline{w'^2}}\sqrt{\overline{\theta_l'^2}})}{\tilde{w}_1}. \quad (7)$$

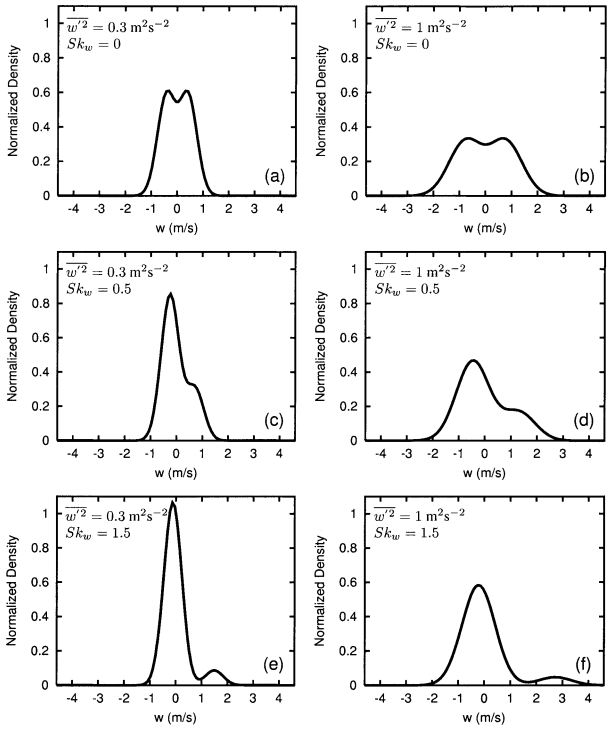

FIG. 1. Examples of double Gaussian PDFs projected to the vertical velocity axis with differing variances and skewnesses. Two variance values ($\overline{w'^2}$ = 0.3, 1 m^2 s^{-2}) and three skewness values ($\mathrm{Sk}_w = \overline{w'^3}/\overline{w'^2}^{1.5}$ = 0, 0.5, 1.5) are shown.

Unlike the widths of the Gaussians along the w axis, the widths along the θ_l axis, $\sigma_{\theta_l 1}$ and $\sigma_{\theta_l 2}$, are allowed to differ. They are computed from the equations for $\overline{\theta_l'^2}$ and $\overline{\theta_l'^3}$. Since $\overline{\theta_l'^3}$ is not a prognostic variable, an additional assumption regarding the skewness of θ_l is needed. We simply assume that it is zero. The procedure to obtain the parameters q_{t1}, q_{t2}, $\sigma_{q_t 1}$, and $\sigma_{q_t 2}$ is similar. The skewness of q_t is assumed to be proportional to Sk_w with a proportionality coefficient of 1.2. We realize that the skewness assumptions made here are not very realistic. Larson et al. (2002) also tested another, more costly, double Gaussian family of PDFs based on Lewellen and Yoh (1993). It does not make such assumptions and was found to perform slightly better than the PDF used here. However, the potential gains come at the price of additional cost and complexity of predicting the third moments of q_t and θ_l. Finally, the subplume correlation $r_{q_t\theta_l}$ is obtained from the $\overline{q_t'\theta_l'}$ equation. Note also that special cases arise when any of the predicted second- or third-order moments are vanishingly small. The procedure in these cases is detailed in Larson et al. (2002).

We now introduce the prognostic equations governing the time evolution of the 10 moments required by the parameterization. Since the parameterization is implemented in a single-column framework, the mean vertical velocity is imposed and does not need to be explicitly prognosed. However, the single-column model does prognose the mean horizontal winds $\overline{u}$ and $\overline{v}$. To derive the predictive equations, we use the filtering approach, in which the model-resolved fields are regarded as a running spatial average of finite width (Germano 1992). As a notational shorthand, we will write $\overline{a'b'}$, but this is meant to be interpreted as $\overline{ab} - \overline{a}\,\overline{b}$, and similarly for other moments. The probability distribution associated with the filtering approach is the probability of finding w, θ_l, and q_t within a *spatially filtered* region. The PDFs referred to in this paper are therefore, strictly speaking, "filtered density functions," as discussed in Colucci et al. (1998).

The filtered equations describing the time evolution of the grid box mean values are

$$\frac{\partial \overline{u}}{\partial t} = -\overline{w}\frac{\partial \overline{u}}{\partial z} - f(v_g - \overline{v}) - \frac{\partial}{\partial z}\overline{u'w'}, \tag{8}$$

$$\frac{\partial \overline{v}}{\partial t} = -\overline{w}\frac{\partial \overline{v}}{\partial z} + f(u_g - \overline{u}) - \frac{\partial}{\partial z}\overline{v'w'}, \tag{9}$$

$$\frac{\partial \overline{q}_t}{\partial t} = -\overline{w}\frac{\partial \overline{q}_t}{\partial z} - \frac{\partial}{\partial z}\overline{w'q_t'} + \left.\frac{\partial \overline{q}_t}{\partial t}\right|_{\mathrm{ls}}, \quad \text{and} \tag{10}$$

$$\frac{\partial \overline{\theta}_l}{\partial t} = -\overline{w}\frac{\partial \overline{\theta}_l}{\partial z} - \frac{\partial}{\partial z}\overline{w'\theta_l'} + \overline{R} + \left.\frac{\partial \overline{\theta}_l}{\partial t}\right|_{\mathrm{ls}}. \tag{11}$$

Here $\overline{R}$ is the radiative heating rate; f the Coriolis parameter; u_g, v_g the geostrophic winds; and $(\partial \overline{q}_t/\partial t)|_{\mathrm{ls}}$ and $(\partial \overline{\theta}_l/\partial t)|_{\mathrm{ls}}$ are large-scale moisture and temperature forcings. The momentum fluxes $\overline{u'w'}$ and $\overline{v'w'}$ are diagnosed as described later in the text.

The time evolution of the second-order turbulent moments is given by equations similar to André et al. (1978), with the following differences: (i) the mean vertical advection terms have been retained for all moments, (ii) the conservative liquid water potential temperature (θ_l) is used as prognostic temperature variable, with the buoyancy related moments written in terms of virtual potential temperature (Bougeault 1981b):

$$\frac{\partial \overline{w'^2}}{\partial t} = -\overline{w}\frac{\partial \overline{w'^2}}{\partial z} - \frac{\partial \overline{w'^3}}{\partial z} - 2\overline{w'^2}\frac{\partial \overline{w}}{\partial z} + \frac{2g}{\theta_0}\overline{w'\theta_v'} - \frac{2}{\rho_0}\overline{w'\frac{\partial p'}{\partial z}} - \epsilon_{ww}, \tag{12}$$

$$\frac{\partial \overline{q_t'^2}}{\partial t} = -\overline{w}\frac{\partial \overline{q_t'^2}}{\partial z} - \frac{\partial \overline{w'q_t'^2}}{\partial z} - 2\overline{w'q_t'}\frac{\partial \overline{q}_t}{\partial z} - \epsilon_{q_t q_t}, \tag{13}$$

$$\frac{\partial \overline{\theta_l'^2}}{\partial t} = -\overline{w}\frac{\partial \overline{\theta_l'^2}}{\partial z} - \frac{\partial \overline{w'\theta_l'^2}}{\partial z} - 2\overline{w'\theta_l'}\frac{\partial \overline{\theta}_l}{\partial z} - \epsilon_{\theta_l\theta_l}, \tag{14}$$

$$\frac{\partial \overline{q_t'\theta_l'}}{\partial t} = -\overline{w}\frac{\partial \overline{q_t'\theta_l'}}{\partial z} - \frac{\partial \overline{w'q_t'\theta_l'}}{\partial z} - \overline{w'q_t'}\frac{\partial \overline{\theta}_l}{\partial z} - \overline{w'\theta_l'}\frac{\partial \overline{q}_t}{\partial z} - \epsilon_{q_t\theta_l}, \tag{15}$$

$$\frac{\partial \overline{w'q_t'}}{\partial t} = -\overline{w}\frac{\partial \overline{w'q_t'}}{\partial z} - \frac{\partial \overline{w'^2 q_t'}}{\partial z} - \overline{w'^2}\frac{\partial \overline{q}_t}{\partial z} - \overline{w'q_t'}\frac{\partial \overline{w}}{\partial z} + \frac{g}{\theta_0}\overline{q_t'\theta_v'} - \frac{1}{\rho_0}\overline{q_t'\frac{\partial p'}{\partial z}} - \epsilon_{wq_t}, \quad (16)$$

$$\frac{\partial \overline{w'\theta_l'}}{\partial t} = -\overline{w}\frac{\partial \overline{w'\theta_l'}}{\partial z} - \frac{\partial \overline{w'^2\theta_l'}}{\partial z} - \overline{w'^2}\frac{\partial \overline{\theta}_l}{\partial z} - \overline{w'\theta_l'}\frac{\partial \overline{w}}{\partial z} + \frac{g}{\theta_0}\overline{\theta_l'\theta_v'} - \frac{1}{\rho_0}\overline{\theta_l'\frac{\partial p'}{\partial z}} - \epsilon_{w\theta_l}, \quad (17)$$

with g the gravity, ρ_0 and θ_0 the reference density and potential temperature, and $\epsilon_{\psi\psi}$ the dissipation terms.

The prognostic equation for the third-order moment of the vertical velocity ($\overline{w'^3}$) differs slightly from the one in André et al. (1978) because the quasi-normal approximation has not been used and therefore the fourth-order moment of the vertical velocity ($\overline{w'^4}$) is left unclosed:

$$\frac{\partial \overline{w'^3}}{\partial t} = -\overline{w}\frac{\partial \overline{w'^3}}{\partial z} - \frac{\partial \overline{w'^4}}{\partial z} + 3\overline{w'^2}\frac{\partial \overline{w'^2}}{\partial z} - 2\overline{w'^3}\frac{\partial \overline{w}}{\partial z} + \frac{3g}{\theta_0}\overline{w'^2\theta_v'} - \frac{3}{\rho_0}\overline{w'^2\frac{\partial p'}{\partial z}} - \epsilon_{www}. \quad (18)$$

Equations (12), (16), and (17) contain pressure correlation terms that must be parameterized. We follow André et al. (1978) who used a formulation based on Rotta (1951) and Launder (1975):

$$-\frac{2}{\rho_0}\overline{w'\frac{\partial p'}{\partial z}} = -\frac{C_4}{\tau_1}\left(\overline{w'^2} - \frac{2}{3}\overline{e}\right) - C_5\left(-2\overline{w'^2}\frac{\partial \overline{w}}{\partial z} + \frac{2g}{\theta_0}\overline{w'\theta_v'}\right) + \frac{2}{3}C_5\left(\frac{g}{\theta_0}\overline{w'\theta_v'} - \overline{u'w'}\frac{\partial \overline{u}}{\partial z} - \overline{v'w'}\frac{\partial \overline{v}}{\partial z}\right), \quad (19)$$

$$-\frac{1}{\rho_0}\overline{q_t'\frac{\partial p'}{\partial z}} = -\frac{C_6}{\tau_2}\overline{w'q_w'} - C_7\left(-\overline{w'q_w'}\frac{\partial \overline{w}}{\partial z} + \frac{g}{\theta_0}\overline{q_w'\theta_v'}\right), \quad (20)$$

$$-\frac{1}{\rho_0}\overline{\theta_l'\frac{\partial p'}{\partial z}} = -\frac{C_6}{\tau_2}\overline{w'\theta_l'} - C_7\left(-\overline{w'\theta_l'}\frac{\partial \overline{w}}{\partial z} + \frac{g}{\theta_0}\overline{\theta_l'\theta_v'}\right), \quad (21)$$

where τ_1 and τ_2 are dissipation timescales described below. The damping constants C_i are also given later in the text.

Because the model does not predict any higher-order moments of the horizontal winds, we assume that the turbulence kinetic energy $\overline{e}$ is proportional to the vertical velocity variance $\overline{w'^2}$:

$$\overline{e} = \frac{3}{2}\overline{w'^2}. \quad (22)$$

With a proportionality coefficient of 3/2, the first term on the right-hand side of (19) effectively drops out. The model results exhibited only moderate sensitivity when various values for the proportionality constant were tested. The same constant was used for all test cases presented in Part II. However, Eq. (22) would not be appropriate for cases where production of turbulence by shear is important.

For the pressure correlation term in Eq. (18), Bougeault (1981b) suggested the addition of a ''rapid'' term to the formulations used by André et al. (1978):

$$-\frac{3}{\rho_0}\overline{w'^2\frac{\partial p'}{\partial z}} = -\frac{C_8}{\tau_{www}}\overline{w'^3} - C_{11}\left(-2\overline{w'^3}\frac{\partial \overline{w}}{\partial z} + \frac{3g}{\theta_0}\overline{w'^2\theta_v'}\right). \quad (23)$$

The dissipation parameterizations for the second-order moments are expressed as

$$\epsilon_{ww} = \frac{C_1}{\tau_1}\overline{w'^2} - \nu_1\nabla_z^2\overline{w'^2}; \quad (24a)$$

$$\epsilon_{q_tq_t} = \frac{C_2}{\tau_1}\overline{q_t'^2} - \nu_2\nabla_z^2\overline{q_t'^2}, \qquad \epsilon_{\theta_l\theta_l} = \frac{C_2}{\tau_1}\overline{\theta_l'^2} - \nu_2\nabla_z^2\overline{\theta_l'^2},$$

$$\epsilon_{q_t\theta_l} = \frac{C_2}{\tau_1}\overline{q_t'\theta_l'} - \nu_2\nabla_z^2\overline{q_t'\theta_l'}; \quad (24b)$$

$$\epsilon_{wq_t} = -\nu_6\nabla_z^2\overline{w'q_t'}, \qquad \epsilon_{w\theta_l} = -\nu_6\nabla_z^2\overline{w'\theta_l'}; \quad (24c)$$

where ∇_z^2 denotes the second-order vertical derivative. The dissipation parameterizations, with the exception of the turbulent fluxes, are composed of two terms: a Newtonian damping term that is inversely proportional to a characteristic dissipation timescale τ_1, and a background diffusion term. The diffusion term was found to be a needed complement since the Newtonian damping term cannot damp small-scale noise. The diffusion term is typically much smaller than all the other terms in the prognostic equation. The dissipation for the fluxes only incorporates a background diffusion term; a damping term is part of the parameterization of the pressure correlation. The timescales τ_i are taken as the ratio of an eddy length scale L_i (see section 3b, below), and a characteristic velocity scale $\sqrt{\overline{e}}$:

$$\tau_i = \begin{cases} \dfrac{L_i}{\sqrt{\overline{e}}}; & \dfrac{L_i}{\sqrt{\overline{e}}} \le \tau_{\max} \\ \tau_{\max}; & \dfrac{L_i}{\sqrt{\overline{e}}} > \tau_{\max} \end{cases} \qquad i = 1, 2. \quad (25)$$

A maximum dissipation time $\tau_{\max}$ of 900 s is imposed in order to prevent the damping terms from becoming too small in regions with little turbulent activity.

When the PDF parameter a defining the relative

weight of each Gaussian is very close to either 0 or 1, instabilities can develop due to large values of the higher-order moments $\overline{w'^2\theta_v'}$ and $\overline{w'^4}$ diagnosed by the closure. It was found that this problem can be overcome by decreasing the dissipation timescale τ_{www} appearing in Eq. (23) relative to the general timescale τ_1 when a is close to 0 and 1:

$$\tau_{www} = \begin{cases} \tau_1\left[1 + 3\left(1 - \dfrac{a - 0.01}{0.04}\right)\right]^{-1}; \\ \qquad 0.01 \le a < 0.05 \\ \tau_1; \qquad 0.05 \le a \le 0.95 \\ \tau_1\left[1 + 3\left(1 - \dfrac{0.99 - a}{0.04}\right)\right]^{-1}; \\ \qquad 0.95 < a \le 0.99. \end{cases} \tag{26}$$

This modification effectively decreases the dissipation timescale in the predictive equation for $\overline{w'^3}$ by up to a factor of four when a is close to either 0 or 1. The PDF closure enforces that a must lie in the range of 0.01 to 0.99 (Larson et al. 2002).

Finally, the dissipation parameterization for the third-order moment of the vertical velocity $\overline{w'^3}$ is of the form

$$\epsilon_{www} = -(K_w + \nu_8)\nabla_z^2\overline{w'^3}. \tag{27}$$

Compared to the dissipation for the second-order moments [Eq. (24)], a larger diffusion coefficient was found to be necessary to maintain stability of the model. The eddy diffusivity coefficient K_w is

$$K_w = 0.22L_1\overline{e}^{1/2}. \tag{28}$$

The constant appearing in Eq. (28) is comparable to the one used by Moeng and Randall (1984) to damp oscillations appearing near the boundary layer inversion.

The traditional closure problem is regarded as closing the higher-order terms appearing in the predictive moment equations. For the set of equations (12)–(18), they are $\overline{w'q_t'^2}$, $\overline{w'\theta_l'^2}$, $\overline{w'q_t'\theta_l'}$, $\overline{w'^2q_t'}$, $\overline{w'^2\theta_l'}$, and $\overline{w'^4}$. Additionally, buoyancy terms ($\overline{w'\theta_v'}$, $\overline{q_t'\theta_v'}$, $\overline{\theta_l'\theta_v'}$, $\overline{w'^2\theta_v'}$) must also be related to prognostic quantities. This has frequently been regarded as distinct from the closure problem. However, the assumed PDF method allows us to close all those terms in a consistent manner directly from the PDF.

The higher-order moments that need to be closed are computed by integration over the PDF as in Eq. (1). For the analytic double Gaussian 1 PDF family, we obtain after integration

$$\overline{w'\theta_l'^2} = a(w_1 - \overline{w})[(\theta_{l1} - \overline{\theta}_l)^2 + \sigma_{\theta_{l1}}^2] + (1 - a)(w_2 - \overline{w})[(\theta_{l2} - \overline{\theta}_l)^2 + \sigma_{\theta_{l2}}^2], \tag{29}$$

$$\overline{w'^2\theta_l'} = a[(w_1 - \overline{w})^2 + \sigma_{w1}^2](\theta_{l1} - \overline{\theta}_l) + (1 - a)[(w_2 - \overline{w})^2 + \sigma_{w2}^2](\theta_{l2} - \overline{\theta}_l), \tag{30}$$

$$\overline{w'q_t'\theta_l'} = a(w_1 - \overline{w}) \times [(q_{t1} - \overline{q}_t)(\theta_{l1} - \overline{\theta}_l) + r_{q_t\theta_l}\sigma_{\theta_{l1}}\sigma_{q_{t1}}] + (1 - a)(w_2 - \overline{w}) \times [(q_{t2} - \overline{q}_t)(\theta_{l2} - \overline{\theta}_l) + r_{q_t\theta_l}\sigma_{\theta_{l2}}\sigma_{q_{t2}}], \tag{31}$$

and

$$\overline{w'^4} = a[(w_1 - \overline{w})^4 + 6(w_1 - \overline{w})^2\sigma_{w1}^2 + 3\sigma_{w1}^4] + (1 - a)[(w_2 - \overline{w})^4 + 6(w_2 - \overline{w})^2\sigma_{w2}^2 + 3\sigma_{w2}^4]. \tag{32}$$

Expressions for $\overline{w'q_t'^2}$ and $\overline{w'^2q_t'}$ are similar to Eqs. (29) and (30), respectively. In order to compute the buoyancy terms ($\overline{w'\theta_v'}$, $\overline{q_t'\theta_v'}$, $\overline{\theta_l'\theta_v'}$, $\overline{w'^2\theta_v'}$), we first rewrite them as (Bougeault 1981b)

$$\overline{\chi'\theta_v'} = \overline{\chi'\theta_l'} + \frac{1 - \epsilon_0}{\epsilon_0}\theta_0\overline{\chi'q_t'} + \left[\frac{L_v}{c_p}\left(\frac{p_0}{p}\right)^{R_d/c_p} - \frac{1}{\epsilon_0}\theta_0\right]\overline{\chi'q_l'}, \tag{33}$$

where χ' represents w', q_t', θ_l', or w'^2. Here, $\epsilon_0 = R_d/R_v$, R_d is the gas constant of dry air, R_v is the gas constant of water vapor, L_v is the latent heat of vaporization, c_p is the heat capacity of air, and p_0 is a reference pressure. The correlations involving liquid water ($\overline{\chi'q_l'}$) can be computed for a given family of PDFs (Larson et al. 2002).

As currently formulated, the PDF family does not include the horizontal winds u and v as independent variables. Therefore, we use a traditional downgradient approach to close the momentum fluxes appearing in Eqs. (8) and (9):

$$\overline{u'w'} = -K_m\frac{\partial\overline{u}}{\partial z}, \tag{34a}$$

$$\overline{v'w'} = -K_m\frac{\partial\overline{v}}{\partial z}, \tag{34b}$$

where the turbulent transfer coefficient K_m is given by

$$K_m = c_K L_1\overline{e}^{1/2}, \tag{35}$$

with $c_K = 0.548$ as in Duynkerke and Driedonks (1987).

The specific values of the constants C_i and ν_i are as follows: $C_1 = 1.7$, $C_2 = 1.04$, $C_4 = 4.5$, $C_5 = 0$, $C_6 = 4.85$, $C_7 = 0.8$, $C_8 = 2.73$, $C_{11} = 0.2$, $\nu_1 = \nu_2 = \nu_8 = 20\ \text{m}^2\ \text{s}^{-1}$, and $\nu_6 = 30\ \text{m}^2\ \text{s}^{-1}$. Compared to the values suggested by Bougeault (1981b), C_4, C_5, C_6 are identical; C_2, which controls the damping terms on the variances, was reduced by 20% to bring the variances in cumulus layers more in line with large eddy simulation (LES) results; C_7 was also adjusted to improve the magnitude of the turbulent fluxes as compared to the LES; C_8 was reduced; and C_{11} was set to the value suggested by André et al. (1982). Bougeault (1981b)

selected the constants C_8 and C_{11} to artificially reduce the magnitudes of the third-order moments as compared to the LES, because he found ''that large values of the third-order moments lead almost systematically to instability.'' He speculated that ''a possible lack of consistency between the quasi-Gaussian assumption and the non-Gaussian cloud parameterization may be responsible for this instability.'' Although the assumed PDF method does not get rid of all sources of instability, it avoids this particular inconsistency, and we found it necessary to adjust the values of C_8 and C_{11} to obtain realistic values of $\overline{w'^3}$.

b. Eddy length formulation

To compute the dissipation timescale τ or the eddy diffusivity coefficients K_w and K_m, we need to calculate eddy length scales L_1 and L_2. To do so, we adopt the method of Bougeault and André (1986) and Bechtold et al. (1992). They construct L from an upward free path $L_{\rm up}(z)$ and a downward free path $L_{\rm down}(z)$. They let $L_{\rm up}(z) > 0$ be the distance that a parcel at altitude z can be carried upwards by buoyancy until it overshoots and exhausts its initial kinetic energy. The initial kinetic energy is approximated as the turbulence kinetic energy $\overline{e}(z)$ [Eq. (22)]. Therefore,

$$-\int_z^{z+L_{\rm up}} \frac{g}{\overline{\theta}_v(z')}[\overline{\theta}_v(z) - \overline{\theta}_v(z')]\, dz' = \overline{e}(z). \quad (36)$$

Similarly, $L_{\rm down}(z) > 0$ is the distance that a parcel can travel downwards under the influence of buoyancy:

$$\int_{z-L_{\rm down}}^{z} \frac{g}{\overline{\theta}_v(z')}[\overline{\theta}_v(z) - \overline{\theta}_v(z')]\, dz' = \overline{e}(z). \quad (37)$$

Then L must be written as some average of $L_{\rm up}$ and $L_{\rm down}$. We choose the same average as Bougeault and Lacarrère (1989):

$$L = \sqrt{L_{\rm up}L_{\rm down}}. \quad (38)$$

When L is large, turbulence is weakly damped; when L is small, turbulence is strongly damped. Equation (38) ensures that L tends to become small if either $L_{\rm up}$ or $L_{\rm down}$ becomes small.

We modify these formulas to make them more appropriate for cumulus layers. The formulas for $L_{\rm up}$ and $L_{\rm down}$ assume that a parcel is lifted without condensation or dilution. In a cumulus layer, however, this leads to unrealistically low values of $L_{\rm up}$. To increase the upward free path, we assume that the parcel is moist and entraining. That is, we replace (36) with

$$-\int_z^{z+L_{\rm up}} \frac{g}{\overline{\theta}_v(z')}[\theta_{v,\rm parcel}(z') - \overline{\theta}_v(z')]\, dz' = \overline{e}(z), \quad (39)$$

where $\theta_{v,\rm parcel}$ is the virtual potential temperature of a parcel that starts its ascent with the mean value of θ_v at altitude z and entrains with fractional entrainment rate $\mu = (1/M)dM/dz$. Here, M is the mass of the parcel, and we choose $\mu = 6 \times 10^{-4}$ m^{-1}. The calculation of $\theta_{v,\rm parcel}$ assumes that condensation occurs when the parcel exceeds saturation. Lappen and Randall (2001b) also include condensation effects in L.

Despite this modification, our experience is that Eq. (39) still appears to underestimate $L_{\rm up}$ in cumulus layers. This is probably because Eq. (39) represents a ''local'' length scale, whereas for cumulus layers in particular a ''nonlocal'' length scale may be more appropriate. By a local length scale, we mean that Eq. (39) assumes that $L_{\rm up}(z)$ is determined by lifting a parcel with the *mean* value of θ_v at the *local* altitude z. In some cases, parcels initiated in the cumulus layer with $\theta_v = \overline{\theta}_v(z)$ may ascend little if at all, whereas parcels initiated at the ground with $\theta_v = \overline{\theta}_v(0)$ may reach a much higher altitude than z. This reflects the difficulty of defining a general estimate of L. In these cases, it seems reasonable to base the length scale at z on the displacement of parcels lifted from lower levels. Therefore, we use the following procedure to make the length scale nonlocal. After computing $L_{\rm up}(z)$, we find the highest altitude $a_{\rm max} = z'' + L_{\rm up}(z'')$ attained by all parcels lifted from lower altitudes $z'' < z$. If $a_{\rm max}$ exceeds the altitude attained by the parcel started at z—that is, if $a_{\rm max} > z + L_{\rm up}(z)$—then we set $L_{\rm up}(z) = a_{\rm max} - z$. Then $L_{\rm up}$ equals the highest distance above z reached by parcels ascending through z from below. We follow an analogous procedure to nonlocalize $L_{\rm down}$. We can calculate nonlocal versions of $L_{\rm up}$ and $L_{\rm down}$ without adding loops in the computer code beyond those needed to calculate the local $L_{\rm up}$ and $L_{\rm down}$.

Finally, we limit the values of L as follows. Following Bechtold et al. (1992), we set a lower limit $L_{\rm min}$ on $L_{\rm up}$ and $L_{\rm down}$. We choose $L_{\rm min} = 20$ m so that it is smaller than the vertical grid spacing. Also, instability can develop if L is too large. Therefore, we set upper limits on L_1 and L_2:

$$L_1 = \min(L, 400 \text{ m}), \quad \text{and} \quad (40)$$

$$L_2 = \min(L, 2000 \text{ m}). \quad (41)$$

We have found that using different maximum values for L_1 and L_2 mitigates numerical instability. The same maximum length scales are used in all simulations. It might, however, be more judicious to let the maximum values scale with the boundary layer depth.

c. Numerical discretization

Equations (8)–(18) are discretized on a vertically staggered grid as shown in Fig. 2. First- and third-order moments are located at grid box centers (zt levels), whereas second-order and fourth-order moments reside on grid box edges (zm levels). The staggering simplifies the spatial discretization of the prognostic equations; turbulent advection terms, such as $\partial\overline{w'^3}/\partial z$ and $\partial\overline{w'^4}/\partial z$ appearing in the predictive equations for $\overline{w'^2}$ and $\overline{w'^3}$, can be computed directly with a centered-in-space dif-

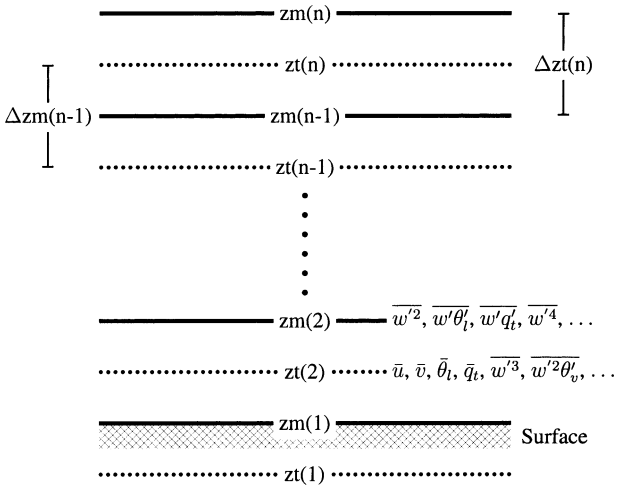

FIG. 2. Model grid setup. The surface is located at the zm(1) level. First- and third-order moments reside on zt levels, and second- and fourth-order moments on zm levels.

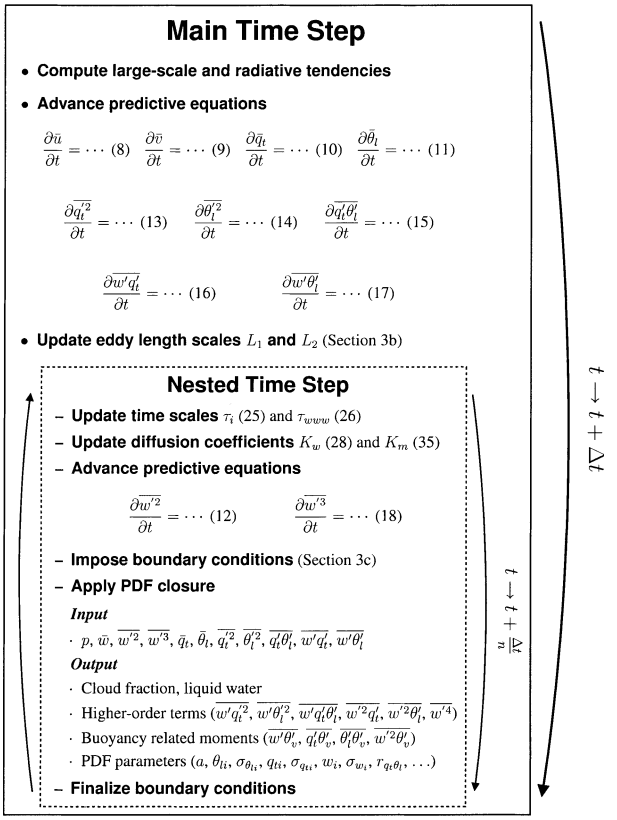

FIG. 3. Schematic representation of the model time step. Numbers in parentheses refer to the equations in the text, Δt is the main time step, and n the time-stepping ratio for the nested time step.

ference without any interpolation. The production terms ($\overline{w'^2}\ \partial\overline{q}_t/\partial z$, . . .) in the second-order moment equations can also be discretized without interpolation. Advection by the mean flow terms ($\overline{w}\ \partial\overline{w'^2}/\partial z$, . . .) require interpolation from the zm levels to the zt levels or vice versa, which is done using a linear scheme. The PDF closure algorithm is applied at the grid box centers (zt levels); the second-order moments are thus interpolated to the zt levels on input to the PDF closure and the fourth-order moment of the vertical velocity ($\overline{w'^4}$) is interpolated back to the zm levels after output from the PDF closure.

The time discretization uses a nested time step. A short time increment is used to integrate the equations involving the higher-order vertical velocity moments [Eqs. (12) and (18)], while all the other moment equations are integrated on the regular time step. This makes it possible to significantly increase the main model time step without causing instability. The time-stepping method is explicit, forward in time, for all terms except for the dissipation terms, which are treated implicitly. The horizontal momentum fluxes are also computed implicitly.

Because of the staggered grid configuration, we only need to impose surface boundary conditions for the second- and fourth-order moments. The turbulent fluxes of momentum ($\overline{u'w'}$, $\overline{v'w'}$), heat ($\overline{w'\theta_l'}$), and moisture ($\overline{w'q_t'}$) can either be imposed or computed using a bulk aerodynamic formula. The surface values of the variances ($\overline{w'^2}$, $\overline{\theta_l'^2}$, $\overline{q_t'^2}$) are computed as in André et al. (1978). The PDF closure scheme is also called at the surface to obtain a boundary condition for $\overline{w'^4}$ and the second-order buoyancy moments. As input, it uses surface values for the second-order moments and interpolated values from the first level above ground for the means and third-order moments. At the upper boundary, all turbulent moments are set to zero since this level is located high enough above the top of the atmospheric boundary layer.

Finally, Fig. 3 gives a visual summary of the various steps involved within each model time step. The model starts by computing large-scale forcings such as advective and radiative tendencies. Equations for the means, as well as equations for the second-order moments with the exception of the vertical velocity variance, are then advanced by one time increment. The eddy length scale is then updated using the new mean profiles. The nested time step follows; it updates the dissipation time and diffusivity coefficients, advances the predictive equations for $\overline{w'^2}$ and $\overline{w'^3}$, imposes boundary conditions and calls the PDF closure scheme to close all higher-order and buoyancy terms. The nested time step procedure is typically repeated between five and seven times within each main model time step.

4. Conclusions

A new cloudy boundary layer single-column model is described that utilizes a joint PDF for representing the subgrid-scale variability of vertical velocity, temperature, and moisture content. The PDF representation is incorporated into a higher-order turbulence closure

scheme and is used to close all higher-order and buoyancy terms, as well as to diagnose cloud fraction and liquid water, all in a manner consistent with the PDF. For each grid point and time step, a particular PDF is selected from an underlying family of PDFs, therefore allowing the PDF to vary in space and evolve in time.

The family of PDFs used in this work is the analytic double Gaussian 1 proposed by Larson et al. (2002). It is based on aircraft observations and LES model outputs of various types of boundary layer clouds, including shallow cumulus and stratocumulus clouds. This family of PDFs depends on 10 free parameters. The values of these parameters are determined from the grid box mean values of the vertical velocity ($\overline{w}$), liquid water potential temperature ($\overline{\theta}_l$), total water specific humidity ($\overline{q}_t$), the six second-order moments ($\overline{w'\theta_l'}$, $\overline{w'q_t'}$, $\overline{q_t'\theta_l'}$, $\overline{w'^2}$, $\overline{\theta_l'^2}$, $\overline{q_t'^2}$), and the third-order moment of the vertical velocity ($\overline{w'^3}$). Filtered Navier–Stokes prognostic equations are integrated to yield the time evolution of these moments. The assumed PDF method can be summarized in three major steps that need to be carried out for each model time step and at each grid box:

1) predict mean quantities and higher-order turbulent moments;
2) use the predicted moments to select a particular PDF member from the family of PDFs;
3) use the particular PDF selected to close higher-order moments and diagnose the buoyancy terms, cloud fraction, and cloud water.

This is detailed in Fig. 3. In Part II (Golaz et al. 2002), we present results obtained with the model described herein for a variety of boundary layer regimes, such as a dry convective layer, trade wind cumulus, cumulus clouds over land, and stratocumulus clouds. These results demonstrate the potential of the PDF-based parameterization approach. We show that, given a family of PDFs that is sufficiently flexible and realistic, it is possible to construct a single scheme capable of simulating very different boundary layer regimes.

Acknowledgments. We are especially thankful to C.L. Lappen for reading and suggesting improvements to this manuscript. We are also grateful to three anonymous reviewers for their valuable comments and suggestions. J.-C. Golaz and W. R. Cotton were supported by the National Science Foundation under Grants ATM-9529321 and ATM-9904218. V. E. Larson was supported by the National Oceanic and Atmospheric Administration under Contract NA67RJ0152.

REFERENCES

André, J. C., G. de Moor, P. Lacarrère, and R. du Vachat, 1976a: Turbulence approximation for inhomogeneous flows. Part I: The clipping approximation. *J. Atmos. Sci.,* **33,** 476–481.

——, ——, ——, and ——, 1976b: Turbulence approximation for inhomogeneous flows. Part II: The numerical simulation of a penetrative convection experiment. *J. Atmos. Sci.,* **33,** 482–491.

——, ——, ——, G. Therry, and R. du Vachat, 1978: Modeling the 24-hour evolution of the mean and turbulent structures of the planetary boundary layer. *J. Atmos. Sci.,* **35,** 1861–1883.

——, P. Lacarrère, and K. Traoré, 1982: Pressure effects on triple correlations in turbulent convective flows. *Turbulent Shear Flows 3: Selected Papers from the Third International Symposium on Turbulent Shear Flows,* L. J. S. Bradbury et al., Eds., Springer-Verlag, 243–252.

Arakawa, A., and W. H. Schubert, 1974: Interaction of a cumulus cloud ensemble with the large-scale environment, Part I. *J. Atmos. Sci.,* **31,** 674–701.

Bechtold, P., C. Fravalo, and J. P. Pinty, 1992: A model of marine boundary-layer cloudiness for mesoscale applications. *J. Atmos. Sci.,* **49,** 1723–1744.

——, J. W. M. Cuijpers, P. Mascart, and P. Trouilhet, 1995: Modeling of trade wind cumuli with a low-order turbulence model: Toward a unified description of Cu and Sc clouds in meteorological models. *J. Atmos. Sci.,* **52,** 455–463.

Bougeault, P., 1981a: Modeling the trade-wind cumulus boundary layer. Part I: Testing the ensemble cloud relations against numerical data. *J. Atmos. Sci.,* **38,** 2414–2428.

——, 1981b: Modeling the trade-wind cumulus boundary layer. Part II: A higher-order one-dimensional model. *J. Atmos. Sci.,* **38,** 2429–2439.

——, 1985: The diurnal cycle of the marine stratocumulus layer: A higher-order model study. *J. Atmos. Sci.,* **42,** 2826–2843.

——, and J.-C. André, 1986: On the stability of the third-order turbulence closure for the modeling of the stratocumulus-topped boundary layer. *J. Atmos. Sci.,* **43,** 1574–1581.

——, and P. Lacarrère, 1989: Parameterization of orography-induced turbulence in a mesobeta-scale model. *Mon. Wea. Rev.,* **117,** 1872–1890.

Bray, K. N. C., and P. A. Libby, 1994: Recent developments in the BML model of premixed turbulent combustion. *Turbulent Reacting Flows,* P. A. Libby and F. A. Williams, Eds., Academic Press, 115–151.

Cahalan, R. F., W. Ridgway, W. J. Wiscombe, and T. L. Bell, 1994: The albedo of fractal stratocumulus clouds. *J. Atmos. Sci.,* **51,** 2434–2455.

Chen, C., and W. R. Cotton, 1987: The physics of the marine stratocumulus-capped mixed layer. *J. Atmos. Sci.,* **44,** 2951–2977.

Colucci, P. J., F. A. Jaberi, and P. Givi, 1998: Filtered density function for large eddy simulation of turbulent flows. *Phys. Fluids,* **10,** 499–515.

Cook, A. W., and J. J. Riley, 1994: A subgrid model for equilibrium chemistry in turbulent flows. *Phys. Fluids A,* **6,** 2868–2870.

Donaldson, C., 1973: Construction of a dynamic model of the production of atmospheric turbulence and the dispersal of atmospheric pollutants. *Workshop on Micrometeorology,* D. A. Haugen, Ed., Amer. Meteor. Soc., 313–392.

Duynkerke, P. G., and A. G. M. Driedonks, 1987: A model for the turbulent structure of the stratocumulus-topped atmospheric boundary layer. *J. Atmos. Sci.,* **44,** 43–64.

——, and ——, 1988: Turbulent structure of a shear-driven stratus-topped atmospheric boundary layer: A comparison of model results with observations. *J. Atmos. Sci.,* **45,** 2343–2351.

Frankel, S. H., V. Adumitroaie, C. K. Madnia, and P. Givi, 1993: Large eddy simulation of turbulent reacting flow by assumed PDF methods. *Engineering Applications of Large Eddy Simulations,* Vol. 162, S. A. Ragab and U. Piomelli, Eds., ASME, 81–101.

Germano, M., 1992: Turbulence: The filtering approach. *J. Fluid Mech.,* **238,** 325–336.

Golaz, J.-C., V. E. Larson, and W. R. Cotton, 2002: A PDF-based model for boundary layer clouds. Part II: Model results. *J. Atmos. Sci.,* **59,** 3552–3571.

Gregory, D., and P. R. Rowntree, 1990: A mass flux convection scheme with representation of cloud ensemble characteristics and stability-dependent closure. *Mon. Wea. Rev.,* **118,** 1483–1506.

Hartmann, D. L., M. E. Ockert-Bell, and M. L. Michelsen, 1992: The

effect of cloud type on earth's energy balance: Global analysis. *J. Climate,* **5,** 1281–1304.

Kessler, E., 1969: *On the Distribution and Continuity of Water Substance in Atmospheric Circulations. Meteor. Monogr.,* No. 32, Amer. Meteor. Soc., 84 pp.

Lappen, C.-L., and D. A. Randall, 2001a: Toward a unified parameterization of the boundary layer and moist convection. Part I: A new type of mass-flux model. *J. Atmos. Sci.,* **58,** 2021–2036.

——, and ——, 2001b: Toward a unified parameterization of the boundary layer and moist convection. Part II: Lateral mass exchanges and subplume-scale fluxes. *J. Atmos. Sci.,* **58,** 2037–2051.

——, and ——, 2001c: Toward a unified parameterization of the boundary layer and moist convection. Part III: Simulations of clear and cloudy convection. *J. Atmos. Sci.,* **58,** 2052–2072.

Larson, V. E., R. Wood, P. R. Field, J.-C. Golaz, T. H. Vonder Haar, and W. R. Cotton, 2001a: Small-scale and mesoscale variability of scalars in cloudy boundary layers: One-dimensional probability density functions. *J. Atmos. Sci.,* **58,** 1978–1994.

——, ——, ——, ——, ——, and ——, 2001b: Systematic biases in the microphysics and thermodynamics of numerical models that ignore subgrid-scale variability. *J. Atmos. Sci.,* **58,** 1117–1128.

——, J.-C. Golaz, and W. R. Cotton, 2002: Small-scale and mesoscale variability in cloudy boundary layers: Joint probability density functions. *J. Atmos. Sci.,* **59,** 3519–3539.

Launder, B. E., 1975: On the effects of a gravitational field on the turbulent transport of heat and momentum. *J. Fluid Mech.,* **67,** 569–581.

Lenschow, D. H., 1998: Observations of clear and cloud-capped convective boundary layers, and techniques for probing them. *Buoyant Convection in Geophysical Flows,* E. J. Plate et al., Eds., Kluwer Academic, 185–206.

Lewellen, W. S., and S. Yoh, 1993: Binormal model of ensemble partial cloudiness. *J. Atmos. Sci.,* **50,** 1228–1237.

Lock, A. P., A. R. Brown, M. R. Bush, G. M. Martin, and R. N. B. Smith, 2000: A new boundary layer mixing scheme. Part I: Scheme description and single-column model tests. *Mon. Wea. Rev.,* **128,** 3187–3199.

Lumley, J. L., and B. Khajeh-Nouri, 1974: Computational modeling of turbulent transport. *Advances in Geophysics,* Vol. 18a, Academic Press, 169–192.

Mellor, G. L., 1977: The Gaussian cloud model relations. *J. Atmos. Sci.,* **34,** 356–358.

Moeng, C.-H., and D. A. Randall, 1984: Problems in simulating the stratocumulus-topped boundary layer with a third-order closure model. *J. Atmos. Sci.,* **41,** 1588–1600.

——, and J. C. Wyngaard, 1989: Evaluation of turbulent transport and dissipation closures in second-order modeling. *J. Atmos. Sci.,* **46,** 2311–2330.

O'Brien, E. E., 1980: The probability density function (PDF) approach to reacting turbulent flows. *Turbulent Reacting Flows,* P. A. Libby and F. A. Williams, Eds., Springer-Verlag, 185–218.

Pincus, R., and S. A. Klein, 2000: Unresolved spatial variability and microphysical process rates in large-scale models. *J. Geophys. Res.,* **105,** 27 059–27 065.

Randall, D. A., 1987: Turbulent fluxes of liquid water and buoyancy in partly cloudy layers. *J. Atmos. Sci.,* **44,** 850–858.

——, Q. Shao, and C.-H. Moeng, 1992: A second-order bulk boundary-layer model. *J. Atmos. Sci.,* **49,** 1903–1923.

Rotstayn, L. D., 2000: On the ''tuning'' of autoconversion parameterizations in climate models. *J. Geophys. Res.,* **105,** 15 495–15 507.

Rotta, J., 1951: Statistiche theorie nichthomogener turbulenz. *Z. Phys.,* **129,** 547–572.

Slingo, A., 1990: Sensitivity of the earth's radiation budget to changes in low clouds. *Nature,* **343,** 49–51.

Sommeria, G., and J. W. Deardorff, 1977: Subgrid-scale condensation in models of non-precipitating clouds. *J. Atmos. Sci.,* **34,** 344–355.

Stull, R. B., 1988: *An Introduction to Boundary Layer Meteorology.* Kluwer Academic, 666 pp.

Tiedtke, M., 1989: A comprehensive mass flux scheme for cumulus parameterization in large-scale models. *Mon. Wea. Rev.,* **117,** 1779–1800.

Wyngaard, J. C., O. R. Coté, and K. S. Rao, 1974: Modeling the atmospheric boundary layer. *Advances in Geophysics,* Vol. 18a, Academic Press, 193–211.